Geophys. J. R. astr. Soc. (1969) **17**, 457–487.

Geomagnetic Variations and the Electrical Conductivity of the Upper Mantle

R. J. Banks

(Received 1969 February 12)

Summary

The electrical conductivity of the upper mantle can be determined by comparing the measured response of the Earth to magnetic variations of all frequencies with the theoretical response of particular conductivity distributions. On the basis of a limited amount of data the response has been estimated at frequencies in the range 0·003 to 0·25 c day^{-1}. In this range of the geomagnetic spectrum, line spectra at frequencies of 1 and 2 c yr^{-1} and 1, 2, and 3 cycles per 27 days can be used. Investigations of the continuum spectrum show that it also occurs on a worldwide scale, and must correspond to a real geophysical process. Meaningful estimates of the response can therefore be made over the whole of the frequency range considered. The entire magnetic variation spectrum in the range 2 c yr^{-1} to 0·25 c day^{-1} appears to be generated by fluctuations in the strength of the ring current, and a P_1^0 spherical harmonic adequately describes the variation of the magnetic field over the surface of the Earth.

The theoretical response of Earth models consisting of concentric shells of variable thickness and conductivity has been computed by putting the boundary problem into a form suitable for the application of matrix methods. The observed P_1^0 response of the Earth is compatible with a distribution in which the conductivity increases sharply by two orders of magnitude at a depth of about 400 km. The width of the region in which this jump occurs is not more than 200 km. It seems likely that the sudden increase in conductivity is caused by a phase transition from the olivine to the spinel form of peridotite. On the basis of this assumption, temperatures have been estimated at depths between 300 and 1000 km.

1. Introduction

Variations of the Earth's magnetic field whose origin is external to the Earth induce electric currents in the more highly conducting parts of the mantle. The induced electric currents give rise in their turn to an internal component of the magnetic variations observed at the surface. By separating magnetic variations into parts of internal (*i*) and external (*e*) origin, we can determine the electromagnetic response of the Earth to a particular input (*e*). The ratio of the parts of the magnetic field of internal and external origin is a measure of the response, and is dependent on both the external current system and the distribution of electrical conductivity within the Earth.

The response has been previously determined at a number of discrete frequencies. Lahiri & Price (1939) used the daily variation to estimate the conductivity at depths of up to 1000 km; Eckhardt *et al.* (1963) investigated the magnetic variations with periods of 27 days and 6 months. However, it is clearly desirable that the response should be determined over as wide a range of frequency as possible if better estimates of the conductivity distribution are to be made.

The distribution of conductivity within the Earth is determined by comparing the observed response with the theoretical response of particular Earth models. When this approach is used particular attention has to be paid to the problem of uniqueness. For the conductivity distribution to have real significance, some attempt has to be made to estimate the range of models which have responses compatible with the observations. Once the conductivity has been specified in this way, we can interpret the variation of conductivity with depth in terms of the effects of temperature and pressure on likely mantle materials.

2. The general approach

2.1 *Analysis of the data*

The available geomagnetic data consists of records of the three components H_r, H_θ, H_ϕ (vertical, horizontal north, and horizontal east components) of the Earth's magnetic field as functions of time, recorded at a number of points distributed over the surface of the Earth. For reasons of ease of manipulation, it is more convenient to work in the frequency than in the time domain. The first step, then, is a Fourier or power spectrum analysis of the magnetic records. The techniques of such analysis are described by Blackman & Tukey (1958).

Once the magnetic variations at each observatory have been analysed in terms of frequency, the spatial behaviour can be expressed by expanding each frequency component in a series of spherical harmonics over the surface of the Earth. At the same time the corresponding magnetic potential can be separated into parts of internal and external origin. What remains is a set of coefficients, $i_n^m(f)$ and $e_n^m(f)$, corresponding to each spherical harmonic component at each frequency. The response function

$$Q_n^m(f) = i_n^m(f)/e_n^m(f)$$

summarizes the whole of the magnetic variation data.

2.2 *Interpretation and the problem of uniqueness*

The usual approach to the problem of determining the distribution of electrical conductivity from the response is to compute the theoretical response of model distributions, and to adjust the model until there is agreement with the observational data. We then have to face the possibility that the model whose response fits the observations need not be the only one which does so. However, R. C. Bailey (personal communication) has succeeded in showing that, under certain conditions, the distribution of conductivity is uniquely determined by the response $Q_n^m(f)$. These conditions are:

(1) that the conductivity is nowhere infinite;

(2) the conductivity is a function only of the radial distance from the centre of the Earth;

(3) the response $Q_n^m(f)$ is known for all frequencies, $0 < f < \infty$.

2.3 *Limitations of the data*

Of the above conditions, we can certainly consider the first to be satisfied within the Earth. The other two deserve more careful consideration.

A considerable body of evidence indicates that lateral variations in the structure of the mantle persist to depths of 400 km, and corresponding variations in the distribution of electrical conductivity are likely to exist. The results of a number of investigations of local anomalies of magnetic variations (Rikitake 1966) confirm this idea. In particular, the highly conducting oceans are known to affect magnetic variations with periods as long as a day. However, it seems reasonable to assume that, for periods rather longer than a day, and depths greater than 400 km, the Earth can be treated as a spherically symmetric conductor.

In determining the response $Q_n^m(f)$, we are restricted to the range of frequencies provided by the natural low frequency electromagnetic spectrum. Fig. 1 is a spectrum of the horizontal component of magnetic variations in the frequency range 10^{-3} to 10 c day^{-1}, recorded at a typical mid-latitude observatory. The steep rise in the spectrum at frequencies less than 10^{-3} c day^{-1} is caused by the secular variation. These long period variations are purely internal in origin, and though they can yield estimates of the electrical conductivity of the lower mantle (McDonald 1957; Currie 1968), are irrelevant for our present purpose. Unfortunately, their amplitude is so large that they completely conceal induced variations with periods greater than three years and effectively set a low frequency limit to the estimation of $Q_n^m(f)$. The high frequency limit is set by the considerations discussed in the preceding paragraph. Magnetic variations with periods of less than one day are affected by lateral variations in conductivity, and should be treated with caution. Most observatories tabulate daily mean values, and this seems a reasonable sampling interval to take in order to avoid such difficulties.

The magnetic variation spectrum in the frequency range 10^{-3} to 0·5 c day^{-1} consists of a number of lines superimposed on an approximately white continuum. The lines are at frequencies of 1 and 2 c yr^{-1}, and at $j/27$ c day^{-1}, where $j = 1, 2, 3,$ etc. They have obvious advantages for the estimation of the response. In general they correspond to periodic phenomena, and their mechanism is reasonably well understood. In addition, they guarantee a high signal/noise ratio. Much more care has to be taken in dealing with the continuum. We have to be quite certain that the continuum is generated by a real geophysical process of worldwide extent, and is not the result of instrumental factors, nor a function of the local observatory environment.

The result of these limitations on the data is a loss of uniqueness. A range of conductivity distributions will exist which are compatible with the observed response.

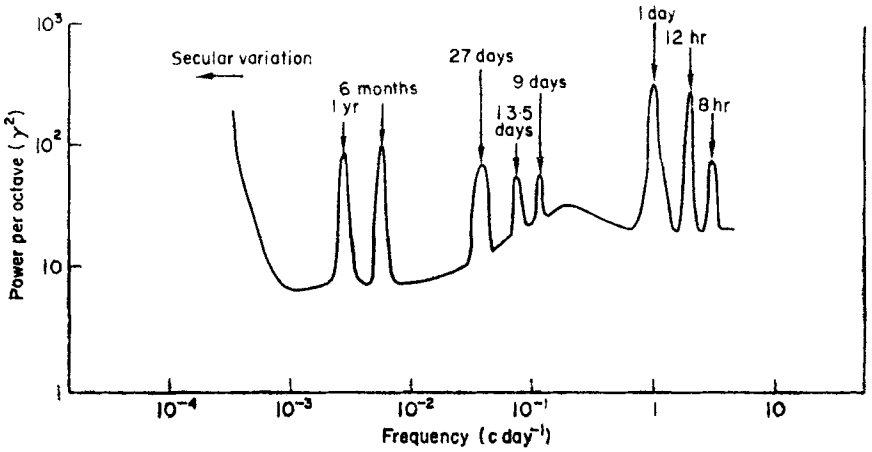

FIG. 1. Power spectrum of the horizontal component of the magnetic field at Greenwich.

An additional source of error is the inaccuracy in the determination of $Q_n^m(f)$. Because of the poor global coverage by observatories, the coefficients of the spherical harmonic expansion, particularly those of the higher harmonics, will be inaccurate.

Part of the difficulty arising from the inadequate distribution of observatories can be overcome by investigating the mechanism responsible for magnetic variations of a particular frequency. The expression of the variations in terms of a series of spherical harmonics is equivalent to a knowledge of the spatial distribution of the current system responsible for the variations. If the nature of the current system is known from other information, there is no need for a formal spherical harmonic expansion. The investigation of the mechanisms responsible for the magnetic variation spectrum is the first step in the analysis of the data.

3. The geomagnetic variation spectrum

3.1 *The 27-day variation and its harmonics*

The 27-day variation can be related to a source on the Sun through the solar rotation period, which varies between 25 days at the solar equator and 30 days at the poles. Furthermore, it has long been known that certain magnetic storms show a tendency to recur at 27-day intervals (Chapman & Bartels 1940).

The source of recurrent magnetic storms is believed to lie in high density, high velocity streams of plasma, originating in regions of the Sun where the magnetic field is weak, uniform, and unidirectional. Associated with the pattern of magnetic fields on the surface of the Sun is a structure in the magnetic field of interplanetary space, generated by the transport of the magnetic field of solar origin by the radially expanding solar wind. This magnetic field structure has been observed to co-rotate with the Sun with a period of 27 days (Wilcox & Ness 1965). The streams of plasma of higher than average velocity and density share the co-rotation, and sweep past the Earth at intervals of 27 days, causing recurrent storms. The orderliness of the co-rotating structure is greatest at sunspot minimum; at the solar maximum the structure is less well defined (Coleman *et al.* 1966). In addition, solar flares are a more important source of high velocity plasma streams at sunspot maximum, and they are generated in regions on the Sun which are characterized by strong, non-uniform magnetic fields. Plasma streams from solar flares are less well organized, and the recurrence tendency is correspondingly less well defined.

The lines in the geomagnetic spectrum at 27 days and its harmonics are caused by the repetition of a basic pattern in the magnetic field. The presence of the harmonics is due to the fact that the repeating unit is not a pure sine wave. However, in order to contribute to the magnetic variation spectrum at 27 days and its harmonics, the repeating unit must itself have components at these frequencies. The repeating unit essentially consists of a single magnetic storm, and the components of the storm which contribute to the low frequency spectrum are the main phase (lifetime approximately 1 day) and the recovery phase (lifetime of 1–20 days). The main phase is caused by the increase in energy of particles in the Van Allen radiation belts. Particles trapped by the geomagnetic field drift round the Earth under the influence of the main dipole field. The resultant ring current produces a magnetic field at the Earth which opposes the dipole field. After the main phase decrease, the magnetic field gradually returns to normal as the ring current decays (Parker 1962).

On this basis, it is clear that the magnetic variations with periods of 27 days etc. are caused by fluctuations in the intensity of the ring current. Until quite recently no direct observations of the ring current during magnetic storms had been made, and there was some doubt as to its location. However, Frank (1966) observed large increases of low energy electron flux at 3–4 R_E (Earth radii) associated with the main phase of a storm. Cahill (1966) detected depressions of the magnetic field at 3–4 R_E

apparently caused by a belt of protons at approximately $3{\cdot}5\,R_E$ from the Earth. Cahill's measurements indicated that the ring current is somewhat asymmetric during the main phase, and is most strongly developed in the evening and night-time sectors. However, the current seems to be much more symmetric during the recovery phase. The mechanism by which the ring current decays is believed to be charge exchange between the protons of the belt and the ambient atomic hydrogen (Parker 1962; Swisher & Frank 1968). The time constant of the recovery phase may therefore be expected to vary, depending on the density of the atomic hydrogen. Johnson (1961) indicates that the hydrogen is three times more dense at $4\,R_E$ during sunspot minimum than it is at sunspot maximum.

The magnetic field perturbation associated with the ring current can be expanded in a series of odd order zonal spherical harmonics. The importance of the $P_3{}^0$ term compared with that of the $P_1{}^0$ term depends on the factor $(R_E/R_R)^2$, where R_E is the radius of the Earth and R_R is the mean radius of the ring current. Because R_R/R_E is approximately 3·5, the $P_3{}^0$ term will contribute less than 10 per cent in an expansion of the ring current field over the surface of the Earth. Terms other than $P_1{}^0$ can therefore be neglected. The work of Eckhardt *et al.* (1963) has shown that a $P_1{}^0$ spherical harmonic is a reasonable single term expression of the latitude dependence of the 27-day variation and its harmonics. They found that the mean square misfit of a $P_1{}^0$ spherical harmonic to the 9-day variation in the horizontal component at a number of observatories was only 2·5 per cent.

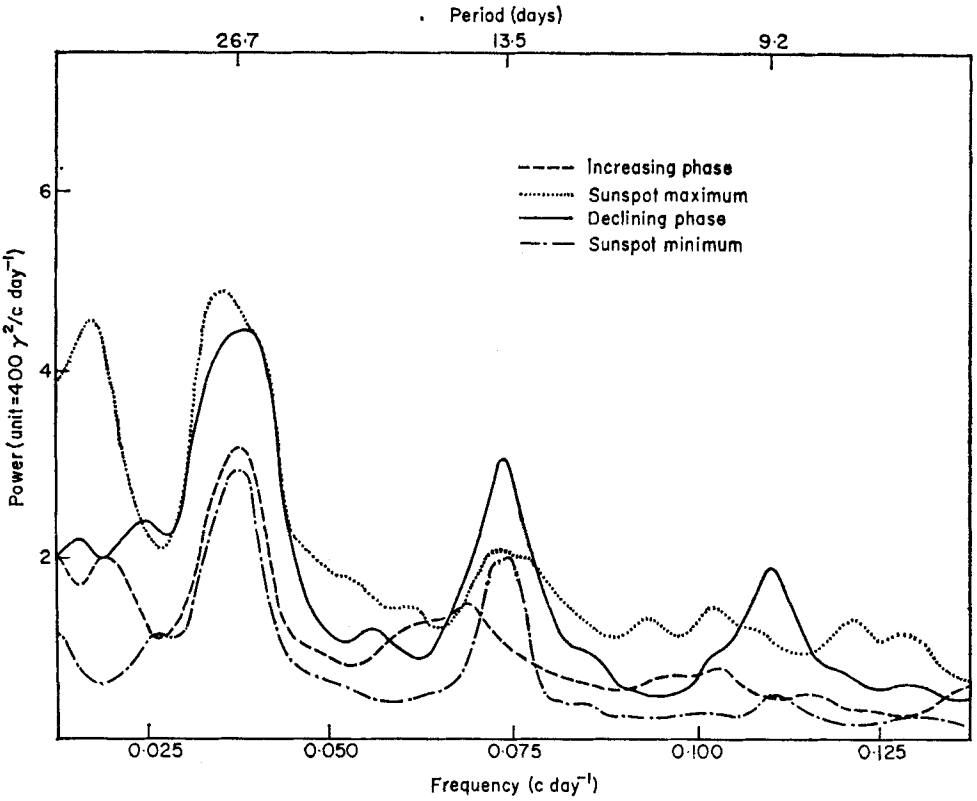

FIG. 2. Power spectra showing the 27-day variation at different levels of solar activity. (Based on 1000-day records of the horizontal field at Greenwich and Abinger; resolution = 1/400 c day^{-1}.)

Because the interplanetary plasma shows greatest order at sunspot minimum, the 27-day variation should be most clearly defined at low levels of solar activity. As a result, the signal/noise ratio of the 27-day variation should depend on the level of solar activity. Fig. 2 is a plot of power spectra of the horizontal component of the magnetic field at Abinger at different phases of solar activity. The magnetic field records were divided up on the basis of the annual mean sunspot numbers, and the plotted spectra represent averages over several solar cycles. Two facts emerge: the width of the 27-day line and its harmonics is least at sunspot minimum, and the harmonics at 13·5 days and 9 days are best defined at low levels of solar activity, The width of the lines is related to the repeatability of the recurring magnetic pattern. and the narrowness of the line at sunspot minimum is most probably due to the greater order of the interplanetary medium at such times. The presence or absence of harmonics, on the other hand, is controlled by the nature of the repeating unit. The small amplitudes of the harmonics at sunspot maximum are probably associated with a slower recovery from the main phase decrease of the storm. Such an explanation supports the ideas of Parker and Johnson that the particles responsible for the decay of the ring current are more dense at sunspot minimum than at sunspot maximum.

In any event, it is apparent from Fig. 2 that the signal/noise ratio of the 27-day variation, and particularly of the harmonics, is greatest during the declining phase of solar activity. By selecting magnetic records corresponding to the declining phase, we can improve the accuracy of the response determination at frequencies of $j/27$ c day^{-1}. The current system responsible for these variations produces a magnetic field at the Earth's surface which can be adequately represented by a P_1^0 spherical harmonic.

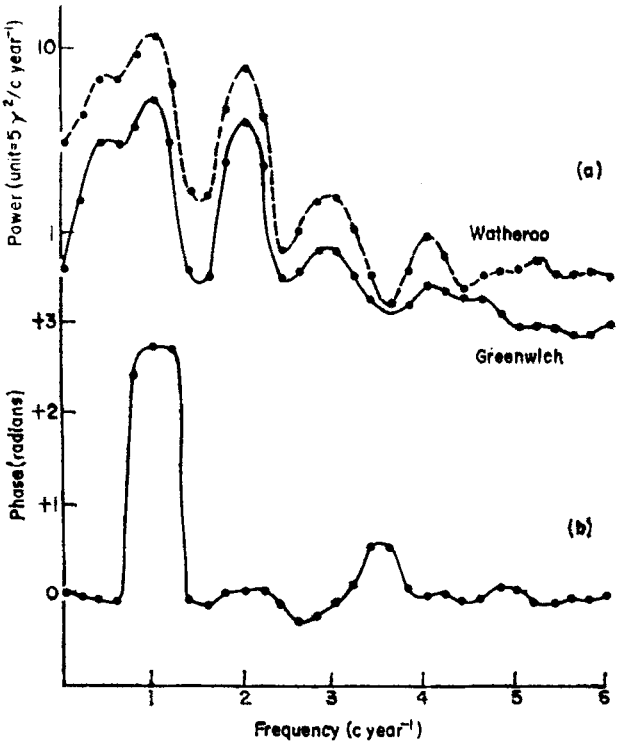

FIG. 3. Power spectra of the horizontal fields at Greenwich and Watheroo: (a) power spectra; (b) phase spectrum. (Based on monthly mean values, 1919–46; resolution = 0·2 c yr^{-1}.)

3.2 *The semi-annual and annual lines*

On the basis of an extensive analysis of magnetic data, Currie (1966) concluded that the annual and semi-annual lines were generated by different mechanisms. His results indicated that an ionospheric dynamo action was probably responsible for the annual variation, while the ring current was the most likely source of the semi-annual line.

The present, less extensive investigation has confirmed Currie's conclusions. Fig. 3 shows power spectra of the horizontal fields at Greenwich and Watheroo for the period 1919–46. The phase difference is zero at a frequency of $2\,\mathrm{c\,yr^{-1}}$, but is 160° at $1\,\mathrm{c\,yr^{-1}}$, clearly indicating the difference between the current systems responsible for the two lines. In Fig. 4, the amplitudes and phases of the horizontal and vertical field variations at $1\,\mathrm{c\,yr^{-1}}$ at a number of stations are plotted as a function of geomagnetic co-latitude. A P_2^0 spherical harmonic seems to fit this limited amount of data quite well. If the ring current can be regarded as the source of the semi-annual variation, as seems likely, a P_1^0 spherical harmonic should be an adequate representation of the magnetic field at the Earth's surface.

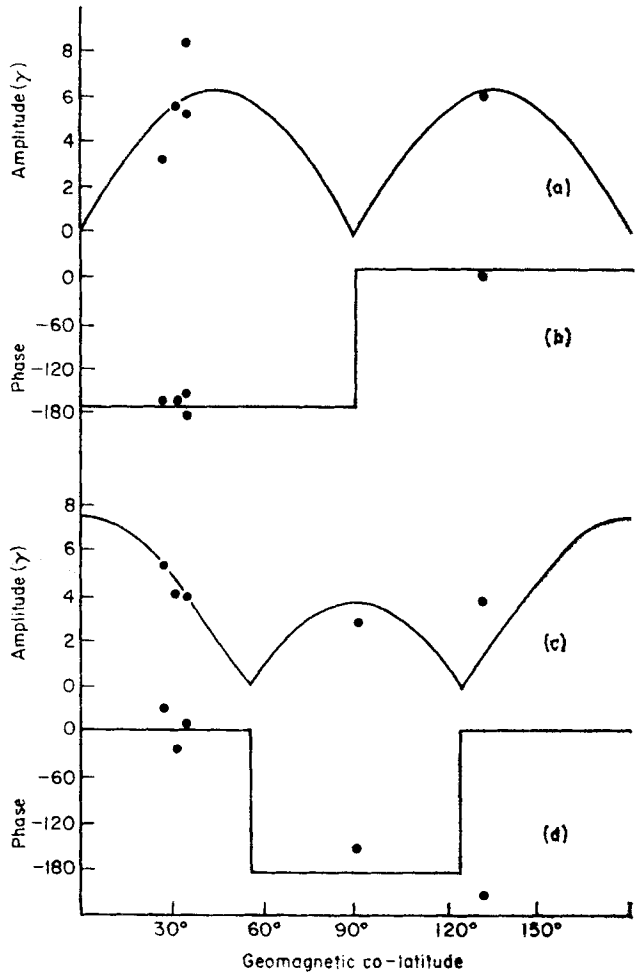

FIG. 4. Latitude dependence of the annual variation: (a) horizontal field amplitudes; (b) horizontal field phases; (c) vertical field amplitudes; (d) vertical field phases. Continuous line is the best least squares fit of P_2^0 to the data.

3.3 *The continuum spectrum*

In Fig. 5, the continuum spectrum in the frequency range 0·05 to 0·5 c day^{-1} is plotted at two different levels of solar activity. Magnetic records (of daily mean values) were selected in 200-day lengths according to sunspot activity, and the results in Fig. 5 represent the average spectra derived from twelve such records. Fig. 5 demonstrates that the level of the continuum power increases by a factor of four at a time when the general magnetic activity is known to increase. An increase of a similar amount is also found in the vertical field power at sunspot maximum. Such results tend to confirm the reality of the continuum, at least during certain phases of solar activity. If we assume that the vertical field power level at sunspot minimum represents an extreme upper bound on instrumental noise, we can guarantee a signal/noise ratio of 2 : 1 in amplitude for the vertical field at sunspot maximum. Because the horizontal field power exceeds the vertical field power by a factor of 10 : 1, the signal/noise ratio for the horizontal field continuum at sunspot maximum must be at least 6 : 1. These estimates of the signal/noise ratio are on the pessimistic side, and can probably be increased by a factor of two.

The worldwide nature of the continuum can be confirmed by investigating the spatial variation of amplitudes, and the cross spectra between widely spaced stations. Fig. 6 shows horizontal field continuum spectra at a number of stations reasonably well distributed in latitude. The spectra are remarkably similar, and there is a clear progression from low horizontal field amplitudes at high geomagnetic latitudes to high amplitudes at low latitudes, suggesting that a P_1^0 spherical harmonic would fit the data quite well. The cross spectra between the horizontal fields at Greenwich

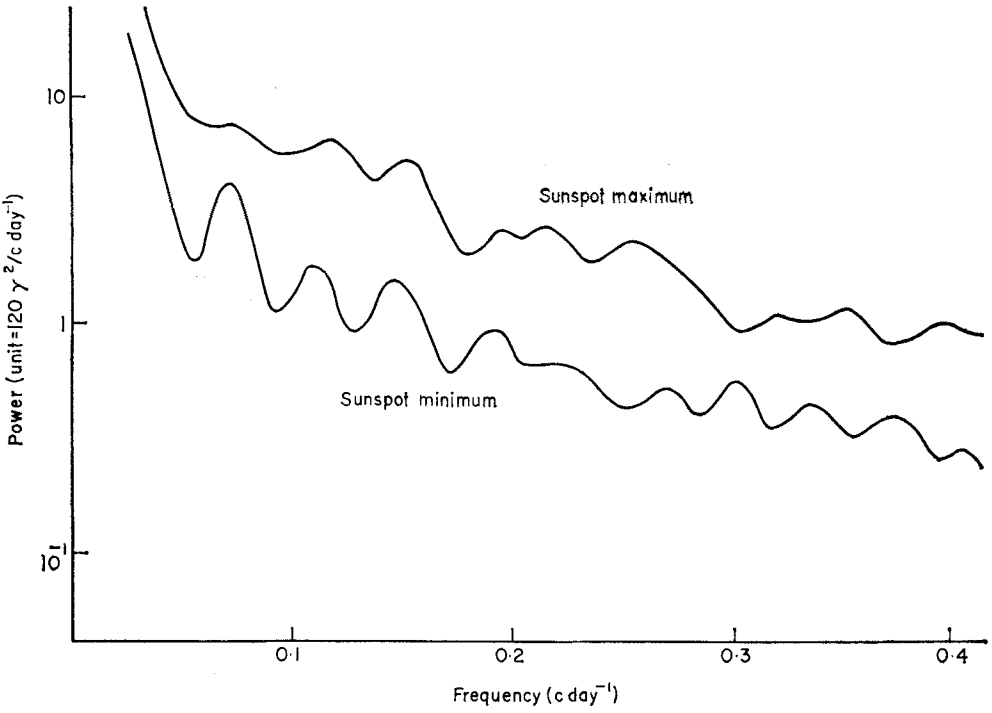

FIG. 5. Average power spectra of the continuum at different levels of solar activity. (Based on 12 200-day records of the horizontal field at Abinger; resolution = 1/120 c day^{-1}.)

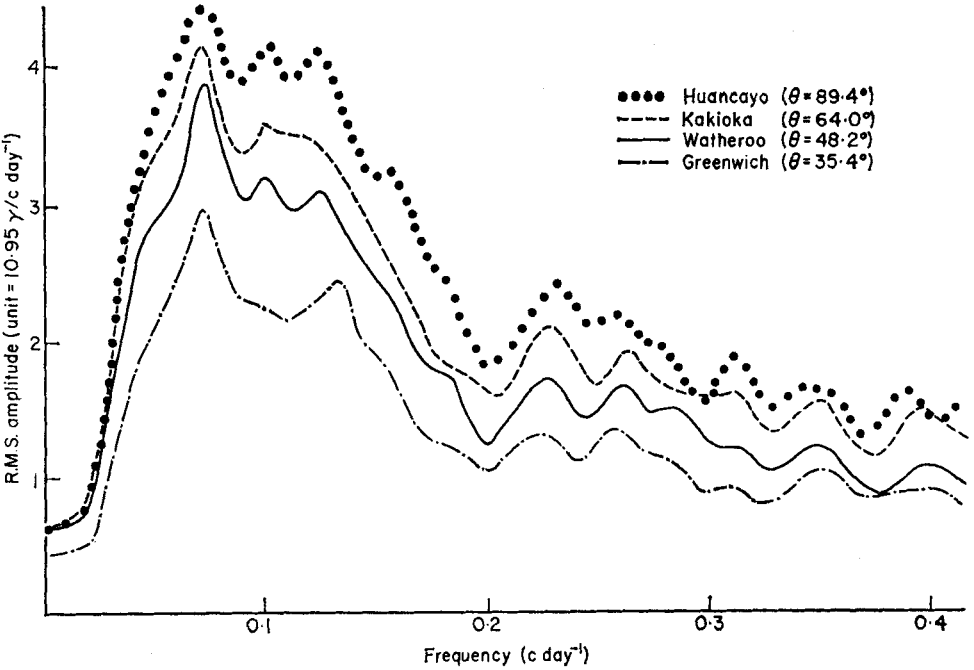

FIG. 6. Amplitude spectra of the horizontal field continuum showing the variation with geomagnetic latitude. (θ = co-latitude relative to nearest pole.)

and Watheroo (Fig. 7) confirm this conclusion. The coherence is high at all frequencies up to 0·25 c day^{-1}, and the phase difference is effectively zero. The vertical field spectra (Fig. 8) are not so satisfactory: the coherence is poor and the phase is unstable.

These results confirm the worldwide nature of the horizontal field continuum and suggest that a P_1^0 spherical harmonic would be an adequate representation. It seems very probable that the continuum is generated either by fluctuations in the negative level of the storm main phase, or by the recovery phase; in other words by fluctuations in the strength of the ring current. This seems to be true for all frequencies between 0·01 and 0·25 c day^{-1}.

The vertical field data is less satisfactory, probably because of the much lower level of vertical field power. Something further has to be done about separating the 'signal' from instrumental noise if satisfactory estimates of the response are to be made.

3.4 *Conclusions*

This brief investigation of the geomagnetic variation spectrum has indicated that the whole of the spectrum between 2 c yr^{-1} and 0·5 c day^{-1} is caused by fluctuations in the intensity of the ring current. The spatial distribution of the associated magnetic field variations at the Earth's surface can be described quite adequately by a P_1^0 spherical harmonic alone. The annual line may be due to an ionospheric dynamo action, and a P_2^0 spherical harmonic is adequate.

The signal/noise ratio of the 27-day variation and its harmonics can be improved by using only data from the declining phase of solar activity; the signal/noise ratio of the continuum is greatest at sunspot maximum.

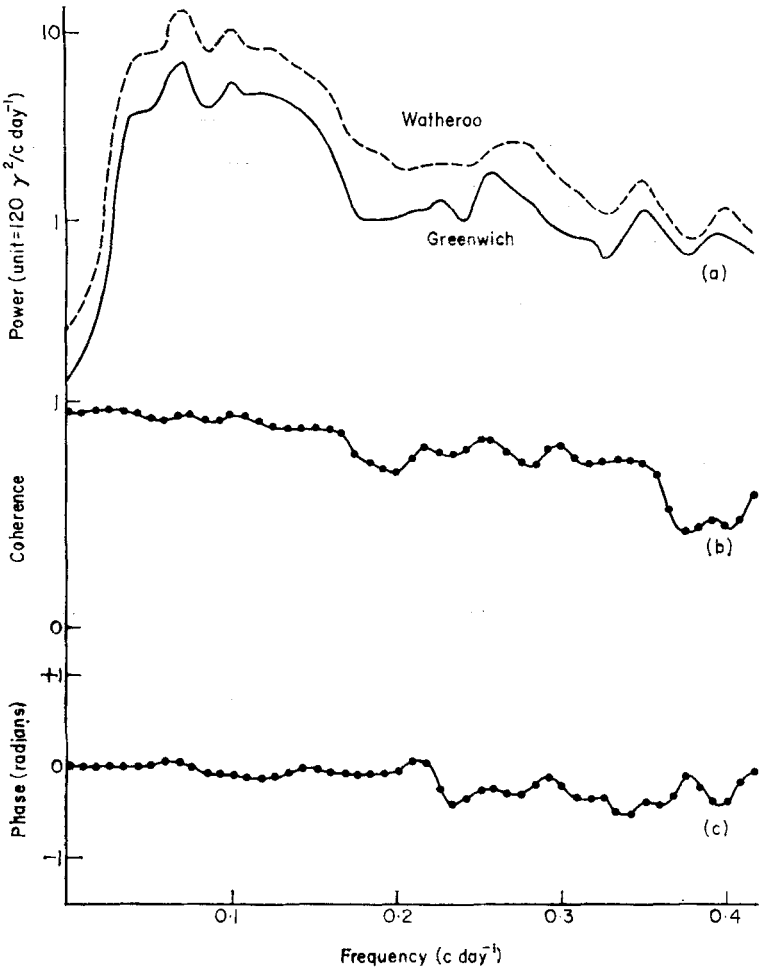

FIG. 7. Power spectra of the horizontal fields at Greenwich and Watheroo: (a) Power spectra; (b) Coherence; (c) Phase. (Based on six 200-day records at sunspot maximum.)

4. Determination of the electromagnetic response of the Earth

The spatial behaviour of magnetic variations in the frequency range $2\,\mathrm{c\,yr^{-1}}$ to $0{\cdot}5\,\mathrm{c\,day^{-1}}$ can be represented by a P_1^0 spherical harmonic. Consequently, the response of the Earth in this range is defined by a single response curve, $Q_1^0(f)$. The theoretical response, $Q_1^0(f)$, of a selected model can be compared with the observations plotted in this way, and the model adjusted until a fit is obtained. The response Q_2^0 at $1\,\mathrm{c\,yr^{-1}}$ can then be computed and compared with the measurements of the annual variation. If necessary the deeper conductivity can be adjusted to fit these observations.

4.1 *The method of calculating the response*

We make the assumption that the magnetic field outside the Earth can be expressed as the gradient of a scalar potential:

$$\mathbf{H} = -\mathrm{grad}\,\Omega. \tag{1}$$

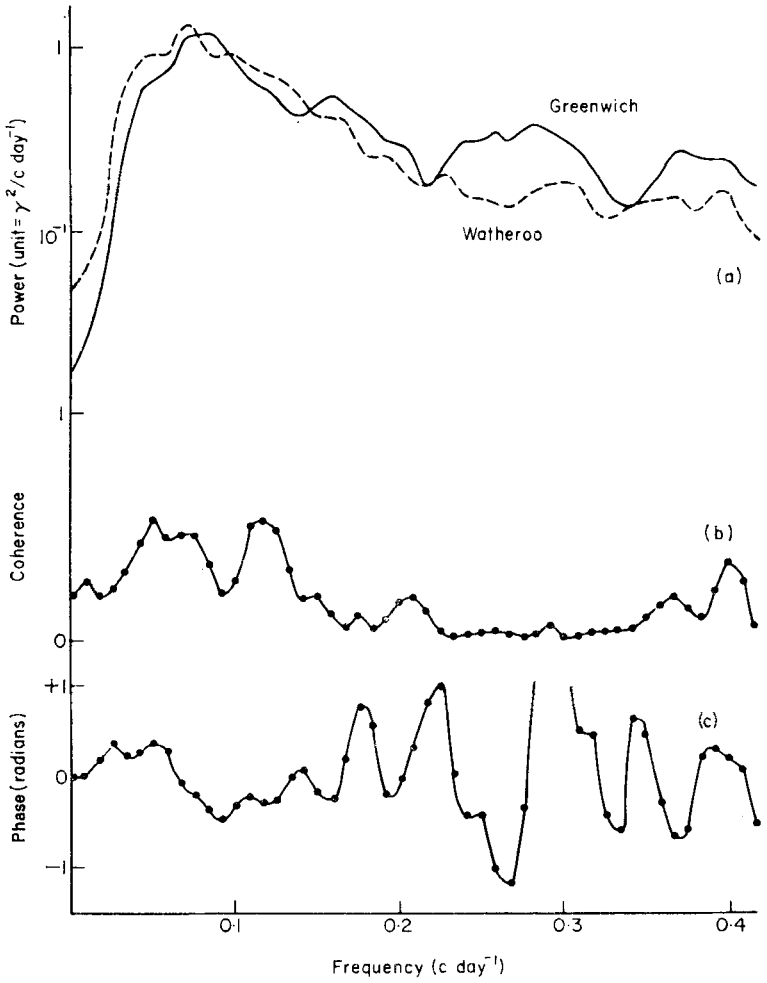

FIG. 8. Power spectra of the vertical fields at Greenwich and Watheroo.

The potential Ω can be expanded as a series of spherical harmonics; in this particular case the harmonics are purely zonal.

$$\Omega = a_0 \sum_n \{i_n(a_0/r)^{n+1} + e_n(r/a_0)^n\} P_n(\cos\theta). \tag{2}$$

The coefficients i_n and e_n, corresponding to the internal and external parts of the field, are complex functions either of time or frequency, depending on the nature of the data. The horizontal (H) and vertical (Z) components of the magnetic field at the Earth's surface ($r = a_0$) are derived from Ω as

$$H = \left(\frac{1}{r}\frac{\partial\Omega}{\partial\theta}\right)_{r=a_0} \tag{3}$$

$$Z = \left(\frac{\partial\Omega}{\partial r}\right)_{r=a_0} \tag{4}$$

For a magnetic variation which can be expressed as a single zonal harmonic of order n, the horizontal and vertical components of the field at co-latitude θ and frequency f can be written as

$$H_n(\theta, f) = A_{H,n}(f)\frac{\partial P_n(\cos\theta)}{\partial\theta} \tag{5}$$

$$Z_n(\theta, f) = A_{Z,n}(f)\, P_n(\cos\theta). \tag{6}$$

It follows from equations (2)–(4) that

$$A_{H,n}(f) = i_n(f)+e_n(f) \tag{7}$$

$$A_{Z,n}(f) = ne_n(f)-(n+1)\, i_n(f). \tag{8}$$

$A_{H,n}(f)$ and $A_{Z,n}(f)$ are determined from the observations by fitting $\partial P_n/\partial\theta$ and P_n to the horizontal and vertical field amplitudes at frequency f by the method of least squares. Equations (7) and (8) can then be used to determine the response function:

$$Q_n(f) = i_n(f)/e_n(f) = \big(n-A_{Z,n}(f)/A_{H,n}(f)\big)\big/\big((n+1)+A_{Z,n}(f)/A_{H,n}(f)\big) \tag{9}$$

However, the results of the response determination indicate that the estimates of the modulus of $W_n(f) = A_{Z,n}(f)/A_{H,n}(f)$ are a good deal more reliable than the estimates of the phase. By calculating $i_n(f)/e_n(f)$, we are introducing uncertainty into both the modulus and phase of $Q_n(f)$. For this reason, it seems preferable to use $W_n(f)$ as the response for the purposes of comparison with theoretical models.

4.2 *The annual line*

The data used in estimating the response at 1 c yr^{-1} has been tabulated by Banks & Bullard (1966). A $P_2{}^0$ spherical harmonic was fitted to the latitude variation by the method of least squares (Fig. 4). The coefficients $A_{H,2}$ and $A_{Z,2}$ were estimated as

$$A_{H,2} = 2{\cdot}11\pm0{\cdot}13\gamma$$

$$A_{Z,2} = 3{\cdot}76\pm0{\cdot}25\gamma$$

giving $$|W_2| = 1{\cdot}78\pm0{\cdot}15 \quad \text{at } 1\,\text{c yr}^{-1}.$$

The mean phase difference, i.e. the phase of W_2, was

$$\alpha_Z-\alpha_H = +170°.$$

4.3 *The semi-annual line*

The only available data which seemed likely, on the basis of signal/noise ratio, to yield a good estimate of W_1 was from a single station—Watheroo. The response was tentatively estimated as $|W_1| = 0{\cdot}45\pm0{\cdot}13$ at 2 c yr^{-1}. The error was calculated from the variance of the spectral estimates (Blackman & Tukey 1958).

4.4 *The 27-day variation and its harmonics*

Data from Greenwich and Watheroo was used in this analysis. Magnetic records were selected to correspond to the declining phase of solar activity, and the spectra were averaged over three or four solar cycles. The response estimates are listed in Table 1.

Table 1

P_1^0 response estimates for the 27-day variation and its harmonics ($\delta|W|$ is the estimated error in $|W|$)

Frequency (c day^{-1})	$\alpha_Z - \alpha_H{}^0$	$\lvert W\rvert$	$\delta\lvert W\rvert$
0·040	162	0·33	0·05
0·073	156	0·26	0·05
0·110	171	0·25	0·05

4.5 *The continuum*

We have seen that the signal/noise ratio of the horizontal field continuum is good, probably 10 : 1 or better. However, for the vertical field continuum it is not so satisfactory, and is probably only 3 : 1 even at sunspot maximum. This estimate of the level of 'instrumental' noise is confirmed by the vertical/horizontal field coherence, which is typically 0·5 to 0·6 at stations at moderate geomagnetic latitudes. If the horizontal field were noise free, while only 70–80 per cent of the vertical field amplitude were 'signal', only 50–60 per cent of the vertical field power would be coherent with the horizontal field, which is what is actually observed.

If we expand the vertical and horizontal field amplitudes at co-latitude θ as a series of zonal spherical harmonics, we can express the ratio $Z(\theta,f)/H(\theta,f)$ as

$$G(\theta,f) = \frac{Z(\theta,f)}{H(\theta,f)} = \frac{\sum_n \{ne_n(f)-(n+1)\,i_n(f)\}\,P_n(\cos\theta)}{\sum_n \{e_n(f)+i_n(f)\}\frac{\partial P_n}{\partial\theta}}. \tag{10}$$

Upon substituting $Q_n(f)\,e_n(f)$ for $i_n(f)$ in equation (10), we obtain the expression

$$G(\theta,f) = \frac{\sum_n e_n(f)\{n-(n+1)\,Q_n(f)\}\,P_n(\cos\theta)}{\sum_n e_n(f)\{1+Q_n(f)\}\frac{\partial P_n}{\partial\theta}}. \tag{11}$$

A high coherence between $Z(\theta,f)$ and $H(\theta,f)$ requires that $G(\theta,f)$ should be stable over the bandwidth of the spectral estimate. From equation (11), we can see that the stability might be affected by:

(1) non-correlated 'instrumental' noise;

(2) changes in the relative amplitudes of the $e_n(f)$ over the bandwidth;

(3) changes in $Q_n(f)$ over the bandwidth of the spectral estimate.

The second and third possibilities can be ruled out: only the e_1 term is likely to be of any importance over a wide range of frequencies, and the response of the Earth, $Q_n(f)$, is not likely to be anything but a smoothly varying function of frequency. The remaining explanation of the poor vertical/horizontal field coherence must be the correct one: i.e. that it is due to uncorrelated 'instrumental' noise in the vertical component.

If both the vertical and horizontal components were noise free, we could write

$$Z(t) = \int_{-\infty}^{+\infty} H(t-\lambda)\,g(\lambda)\,d\lambda \tag{12}$$

where

$$g(\lambda) = \int_{-\infty}^{+\infty} G(f)\exp -i2\pi f\lambda df.$$

However, the vertical field also contains an uncorrelated noise component $n(t)$,

i.e. $$Z(t) = \int_{-\infty}^{+\infty} H(t-\lambda)\, g(\lambda)\, d\lambda + n(t) \tag{13}$$

which becomes, in the frequency domain,

$$Z(f) = H(f)\, G(f) + N(f) \tag{14}$$

where $Z(f)$, $N(f)$ etc. are the Fourier transforms of $Z(t)$, $n(t)$ etc.

The cross spectrum of the observed vertical and horizontal fields, $Z(t)$ and $H(t)$, is

$$C(f) + iD(f) = H(f)\, H^*(f)\, G(f) + N(f)\, H^*(f) \tag{15}$$

where $C(f)$ is the co-spectrum and $D(f)$ the quad-spectrum (Munk & Cartwright 1966); the asterisk denotes a complex conjugate. In order to stabilise the estimates of the cross spectrum, spectra of independent records are averaged, and the individual spectra are smoothed in the frequency domain. Since $n(t)$ and $H(t)$ are uncorrelated, they have random relative phase, and the product $N(f)\, H^*(f)$ averages to zero:

i.e. $$\langle C(f) + iD(f) \rangle = \langle H(f)\, H^*(f) \rangle\, G(f) \tag{16}$$

where the brackets denote average quantities.

Equation (16) provides us with a noise free estimate of $G(f)$, the vertical/horizontal field amplitude ratio at a particular station. Since $P_H(f) = \langle H(f)\, H^*(f) \rangle$ is the power spectrum of the horizontal field, we have

$$G(f) = \frac{\langle C(f) + iD(f) \rangle}{P_H(f)} \tag{17}$$

or alternatively

$$G(f)\, G^*(f) = R^2(f)\, P_Z(f) / P_H(f) \tag{18}$$

where

$$R^2(f) = \frac{|\langle C(f) + iD(f) \rangle|^2}{P_Z(f)\, P_H(f)}$$

is the coherence of the horizontal and vertical fields.

From equation (14) we can calculate the vertical field power spectrum:

$$P_Z(f) = \langle Z(f)\, Z^*(f) \rangle = P_H(f) |G(f)|^2 + P_N(f) \tag{19}$$

which can be written in an alternative form by using equation (18):

$$P_Z(f) = R^2(f)\, P_Z(f) + P_N(f), \tag{20}$$

i.e. the vertical field energy is the sum of the noise power and the coherent vertical field power.

The vertical/horizontal field coherence is computed at each station, and the coherent vertical field amplitude $\sqrt{R^2(f)\, P_Z(f)}$ is calculated. The horizontal field is assumed to be noise free. The coherent vertical field amplitudes and the horizontal field amplitudes are then fitted to a $P_1{}^0$ spherical harmonic by the method of least squares, to obtain noise free estimates of $A_{Z,\,1}(f)$ and $A_{H,\,1}(f)$. Six 200-day records of daily mean values at a time of solar maximum were used in the analysis. Fig. 9 shows the resulting estimates of $A_{Z,\,1}(f)$ and $A_{H,\,1}(f)$.

The fall in the spectra at the low frequency end is due to filtering which was necessary to prevent leakage from the secular variation. The coherence falls to too low a level at frequencies greater than 0·25 c day^{-1} for significant estimates of $A_{Z,\,1}(f)$ to be made. The error bars represent the standard error derived from the least squares misfit, but, because of the small number of stations involved, can only be regarded as rather crude error estimates.

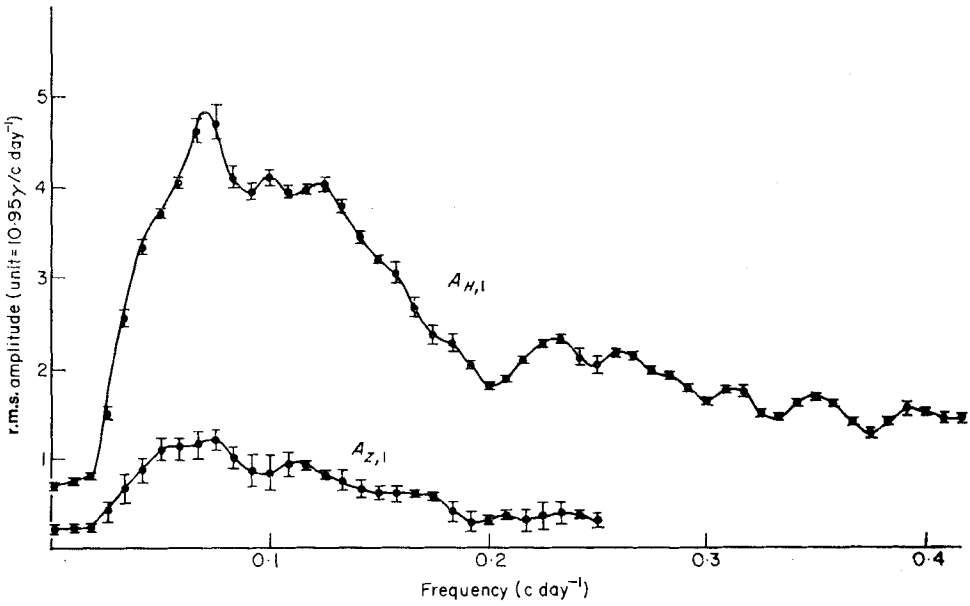

FIG. 9. Noise free estimates of the vertical ($A_{Z,1}$) and horizontal ($A_{H,1}$) r.m.s. amplitudes. (Data from Abinger, Huancayo, Kakioka, Watheroo.)

Similar techniques can be applied to longer stretches of data in order to estimate the response at lower frequencies. The necessary increase in resolution will, however, reduce the certainty in the spectral estimates unless there is a corresponding increase in the amount of data.

4.6 *The overall response*: 2 *c yr*$^{-1}$ *to* 0·25 *c day*$^{-1}$

In Figs 10 and 11 the whole of the $P_1{}^0$ data has been assembled: $|W_1(f)|$ is plotted in Fig. 10, and the phase in Fig. 11. Because the response is quite flat at the high frequency end, it has been possible to further smooth the estimates from the continuum in this region. This was not possible at the low frequency end, where the response appears to rise quite rapidly. The phase estimates appear to exceed 180° at frequencies greater than 0·12 c day^{-1}; the reason for this is not known.

The response estimates from the line spectra have also been plotted for the purpose of comparison with the results from the continuum. The agreement is good, and appears to justify the method of analysing the continuum data that was used.

5. Theoretical calculations of the response

5.1 *The basic equations*

The equation for the electric field **E** that we have to solve is the diffusion equation:

$$\nabla^2 \mathbf{E} = \mu\mu_0 \sigma \frac{\partial \mathbf{E}}{\partial t} \tag{21}$$

in rationalized M.K.S. units (μ is the magnetic permeability and σ the electrical conductivity of the medium. μ_0 is the permeability of free space.) In deriving this equation it is assumed that the volume charge density within the Earth is zero, and that the electromagnetic wave solutions can be neglected (Lahiri & Price 1939).

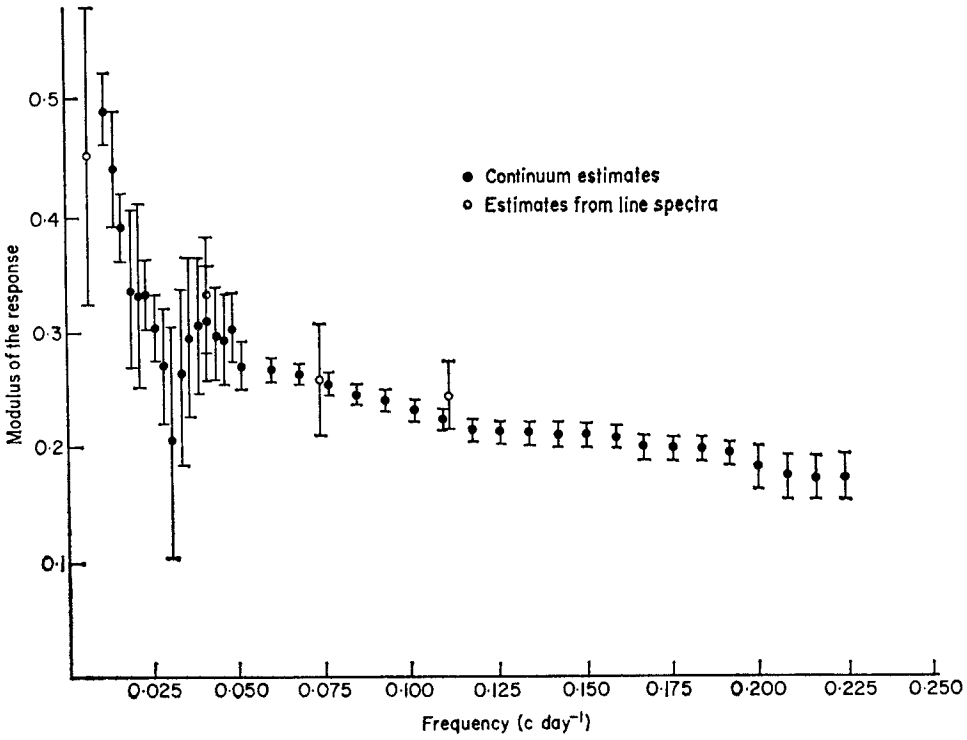

FIG. 10. P_1^0 response estimates: $|W_1^0|$.

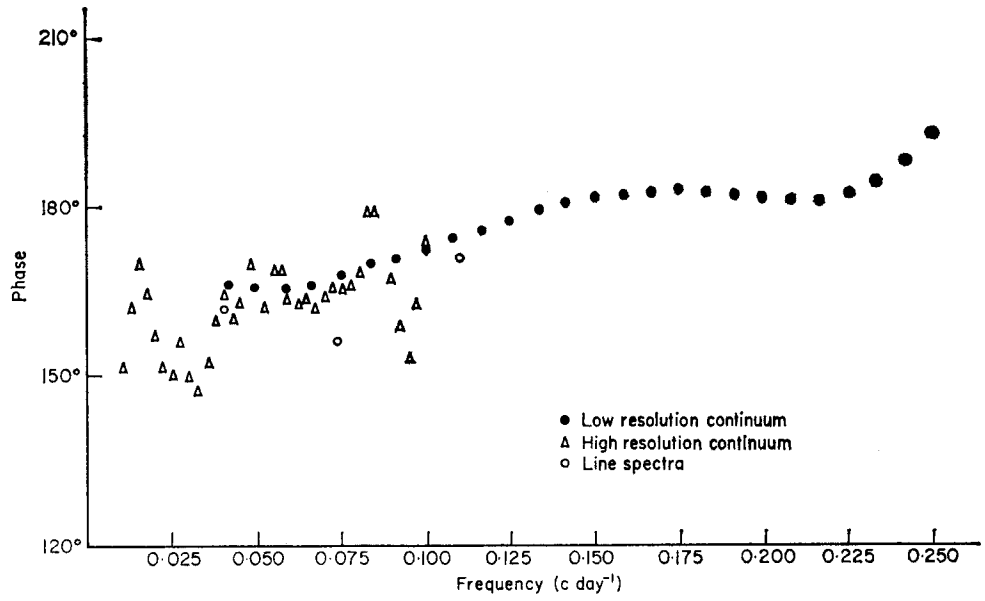

FIG. 11. P_1^0 response estimates: phase.

For a field variation of frequency w, i.e. with a time dependence e^{iwt}, equation (21) becomes

$$\nabla^2 \mathbf{E} + k^2 \mathbf{E} = 0 \tag{22}$$

where

$$k^2 = -iw\mu\mu_0\sigma. \tag{23}$$

The general solution can be formed by superposing solutions for different values of the frequency, w. The magnetic field $\mathbf{B}$ can then be calculated as

$$\mathbf{B} = -\frac{1}{iw}\operatorname{curl}\mathbf{E}. \tag{24}$$

In the following sections it is assumed that $\mu = 1$ throughout the Earth, i.e. that ferromagnetism is not important. Tozer (1959) discusses the validity of this assumption. Finally, the conductivity σ is assumed to be a function of r only, and to be independent of θ and ϕ (see Section 2.3).

5.2 *Solutions of the vector Helmholtz equation*

Stratton (1941) shows that there are three types of solution to equation (22) in spherical co-ordinates. They are

$$\mathbf{T} = \operatorname{curl}(\Psi\mathbf{r})$$

$$\mathbf{S} = \operatorname{curl}\operatorname{curl}(\Phi\mathbf{r})$$

$$\mathbf{U} = -\operatorname{grad}\Omega.$$

and correspond to the toroidal, poloidal, and irrotational vector fields respectively. Ψ, Φ and Ω are scalar functions of r, θ, ϕ.

Inside a conductor, the magnetic field can be expressed completely as a sum of **T** and **S** type solutions. In a region where the conductivity is zero, the field can be represented by a **U** type solution. If the magnetic field outside a conductor is expressed as the gradient of a scalar potential, the boundary conditions are satisfied by a purely poloidal field inside the conductor. Since the electric field can be written as the curl of the magnetic field, the electric field inside the conductor must be toroidal.

By substituting the toroidal **E** field solution into equation (22), we obtain

$$\nabla^2\Psi + k^2\Psi = 0. \tag{25}$$

This equation can be solved by separating the variables:

$$\Psi = \sum_{n=0}^{\infty}\sum_{m=-n}^{+n} R_n(r)\, Y_n^m(\theta,\phi) \tag{26}$$

where the $Y_n^m(\theta,\phi)$ are spherical harmonics, and $R_n(r)$ is a solution of the equation

$$r^2\frac{d^2R_n}{dr^2} + 2r\frac{dR_n}{dr} - (n(n+1) - k^2r^2)\,R_n = 0. \tag{27}$$

The electric field is calculated by using the relation

$$\mathbf{E} = \operatorname{curl}(\mathbf{r}\Psi).$$

The magnetic field is then determined by equation (24). Chandrasekhar (1961) shows that the components of the magnetic field are

$$B_r = -\frac{1}{iw\rho a_0}\sum_{n,m} R_n(\rho)\, n(n+1)\, Y_n^m(\theta,\phi)\, e^{iwt} \tag{28}$$

$$B_\theta = -\frac{1}{iw\rho a_0}\sum_{n,m}\frac{d}{d\rho}\left(\rho R_n(\rho)\right)\frac{\partial Y_n^m}{\partial\theta}(\theta,\phi)\,e^{iwt} \tag{29}$$

$$B_\phi = -\frac{1}{iw\rho a_0\sin\theta}\sum_{n,m}\frac{d}{d\rho}\left(\rho R_n(\rho)\right)\frac{\partial Y_n^m}{\partial\phi}(\theta,\phi)\,e^{iwt} \tag{30}$$

where the substitution $\rho = r/a_0$ has been made (a_0 is the radius of the Earth). The corresponding radial equation is

$$\rho^2\frac{d^2R_n}{d\rho^2} + 2\rho\frac{dR_n}{d\rho} - \left(n(n+1) - k^2a_0^2\rho^2\right)R_n = 0. \tag{31}$$

5.3 *Solutions of the radial equation*

Equation (31) can be solved by dividing the Earth into concentric shells each of different conductivity, the conductivity within any one shell being constant. The substitution of $z = ka_0\rho$ into equation (31) gives

$$z^2\frac{d^2R_n}{dz^2} + 2z\frac{dR_n}{dz} + \left(z^2 - n(n+1)\right)R_n = 0. \tag{32}$$

The general solution of this equation is

$$R_n(z) = \alpha j_n(z) + \beta y_n(z), \tag{33}$$

where $j_n(z)$ and $y_n(z)$ are complex spherical Bessel functions (Abramowitz & Stegun 1965).

5.4 *Boundary conditions*

Within each shell α and β are constant, but they will in general vary from one shell to the next, and the relationship of the values of α and β has to be determined by applying the appropriate boundary conditions. These are that the component of **B** normal to the boundary (B_r), and the component of **B** tangential to the boundary (B_θ or B_ϕ), are both continuous. The second condition holds provided there is no surface current distribution (such as would be the case at the surface of a superconducting shell).

At a boundary $\rho = \rho_1$ between two conducting shells, the condition of continuity of B_r leads to

$$R_{n,1}(\rho_1) = R_{n,2}(\rho_1) \tag{34}$$

where $R_{n,1}(\rho)$ and $R_{n,2}(\rho)$ are solutions of the radial equation in layers 1 and 2 respectively. The continuity of B_θ supplies the condition

$$\rho_1\left(\frac{dR_{n,1}}{d\rho}\right)_{\rho=\rho_1} + R_{n,1}(\rho_1) = \rho_1\left(\frac{dR_{n,2}}{d\rho}\right)_{\rho=\rho_1} + R_{n,2}(\rho_1).$$

Since we already have the condition of equation (34), the extra condition is simply

$$\left(\frac{dR_{n,1}}{d\rho}\right)_{\rho=\rho_1} = \left(\frac{dR_{n,2}}{d\rho}\right)_{\rho=\rho_1}. \tag{35}$$

At the surface of the conductor, the magnetic field solutions (28)–(30) have to be matched to solutions of the **U** type. For a magnetic field variation expressible purely in zonal harmonics, the components of the field outside the conductor are

$$B_r = -\sum_n\left(ne_n\rho^{n-1} - (n+1)i_n\rho^{-(n+2)}\right)P_n\,e^{iwt} \tag{36}$$

and

$$B_\theta = -\sum_n\left(e_n\rho^{n-1} + i_n\rho^{-(n+2)}\right)\frac{dP_n}{d\theta}\,e^{iwt}. \tag{37}$$

The conditions of continuity of B_r and B_θ at the surface of the conductor lead to the relations

$$R_{n,s}(\rho_0) = \frac{iw\rho_0 a_0}{n(n+1)} \left(ne_n \rho_0^{n-1} - (n+1) i_n \rho_0^{-(n+2)}\right) \tag{38}$$

and

$$\left(\frac{d}{d\rho}(\rho R_{n,s}(\rho))\right)_{\rho=\rho_0} = iw\rho_0 a_0 (e_n \rho_0^{n-1} + i_n \rho_0^{-(n+2)}). \tag{39}$$

The surface of the conductor is at $\rho = \rho_0$, and the layer immediately beneath the surface is labelled s.

5.5 *Computational techniques*

The penetration of any magnetic variation into the Earth is limited by the eddy currents set up in the more highly conducting regions of the mantle. The skin depth is a measure of the penetration at a particular frequency. At a depth several times that of the skin depth, the currents associated with a variation at that frequency will be negligible, and the measured response at that frequency will be for all practical purposes independent of the conductivity of deeper layers. For this reason it is possible to take an arbitrary conductivity, either zero or infinity, at a depth well below the skin depth. Because magnetic variations are effectively excluded from a central core, it seems reasonable to treat the Earth as a super-conductor at depths much greater than the skin depth of the lowest frequency considered.

At the surface of a superconducting sphere the component of a magnetic variation normal to the surface (B_r) is zero, while B_θ can take an arbitrary value. From the values of B_r, B_θ at the surface of the core we can compute the magnetic field at the top of the first shell of finite conductivity. By applying the boundary conditions described in Section 5.4 we can work our way through successive shells to the surface, and finally determine $Q_n(f)$ or $W_n(f)$. Such a method of matching boundary values lends itself to the application of matrix methods. A similar approach is used in the Thomas–Haskell method of calculating surface wave dispersion (Anderson 1965).

At a boundary $\rho = \rho_l$ between two conducting layers $l-1$ and l, we can use the boundary conditions (34) and (35) and the explicit solution for $R_n(ka_0\rho)$ given by equation (33) to derive a pair of equations relating α_l and β_l to α_{l-1} and β_{l-1}:

$$\alpha_{l-1} j_n(k_{l-1} a_0 \rho_l) + \beta_{l-1} y_n(k_{l-1} a_0 \rho_l) = \alpha_l j_n(k_l a_0 \rho_l) + \beta_l y_n(k_l a_0 \rho_l)$$

$$\alpha_{l-1} j_n'(k_{l-1} a_0 \rho_l) + \beta_{l-1} y_n'(k_{l-1} a_0 \rho_l) = \alpha_l j_n'(k_l a_0 \rho_l) + \beta_l y_n'(k_l a_0 \rho_l)$$

where

$$j_n'(k_{l-1} a_0 \rho_l) = \left(\frac{d}{d\rho}(j_n(k_{l-1} a_0 \rho))\right)_{\rho=\rho_l} \quad \text{etc.}$$

In matrix terms, these equations can be written as

$$\mathscr{C}(k_{l-1}, \rho_l)\,\mathbf{X}_{l-1} = \mathscr{C}(k_l, \rho_l)\,\mathbf{X}_l = \mathbf{K}_l \tag{40}$$

where

$$\mathscr{C}(k_l, \rho_l) = \begin{pmatrix} j_n(k_l a_0 \rho_l) & y_n(k_l a_0 \rho_l) \\ j_n'(k_l a_0 \rho_l) & y_n'(k_l a_0 \rho_l) \end{pmatrix}$$

$\mathbf{X}_l = \begin{pmatrix} \alpha_l \\ \beta_l \end{pmatrix}$ and $\mathbf{K}_l$ is effectively $\begin{pmatrix} B_r \\ B_\theta \end{pmatrix}$ at the lth boundary.

Having started with a value for $\mathbf{K}$ at the surface of the superconducting core, we wish to transform it by successive matrix operations to the vector $\mathbf{K}$ at the surface

of the Earth, where it can be expressed in terms of i_n and e_n. In general we need a matrix which will transform $\mathbf{K}_l$ into $\mathbf{K}_{l+1}$. From equation (40) it follows that

$$\mathbf{K}_{l+1} = \mathscr{B}(k_l, \rho_l, \rho_{l+1})\,\mathbf{K}_l$$

where
$$\mathscr{B}(k_l, \rho_l, \rho_{l+1}) = \mathscr{C}(k_l, \rho_{l+1})\,\mathscr{C}^{-1}(k_l, \rho_l) \tag{41}$$

$\mathscr{B}$ is the required matrix operator.

The choice of $\mathbf{K}$ at the surface of the superconducting core must be such as to satisfy the boundary condition that the normal component of $\mathbf{B}$ should be zero. Consideration of equations (28)–(29), (34)–(35) indicates that $\mathbf{K} = \begin{pmatrix} 0 \\ 1 \end{pmatrix}$ meets this requirement.

Once the vector $\mathbf{K}$ has been calculated at the surface of the conductor, an additional matrix operation is required to transform $\mathbf{K}$ into the response $\mathbf{Q} = \begin{pmatrix} i_n \\ e_n \end{pmatrix}$. This operation is performed by the matrix

$$\mathscr{A} = \begin{pmatrix} \dfrac{n}{n+1}\,\rho_0{}^{n-1} & -\rho_0{}^{n}/(n+1) \\ -\left(\dfrac{n+1}{n}\right)\rho_0{}^{-(n+2)} & -\rho_0{}^{-(n+1)}/n \end{pmatrix}$$

ρ_0 is the value of ρ at the surface of the conductor (not necessarily the surface of the Earth).

6. The conductivity distribution

The problem with which we are faced is that of finding a distribution of conductivity which has the same $P_1{}^0$ response as the Earth at frequencies between 0·005 and 0·25 c day^{-1}. To save time in examining and discarding models, two other lines of approach can be used. Certain simple conductivity distributions have response curves which can be inverted to yield unique information about the model. The two most important models having this property are the superconducting core model and the uniform core model. By inverting the measured response curve on the assumption that one of these models is a reasonable approximation to the truth, we ought to be able to form some idea of the actual conductivity distribution. The second approach takes as its starting point the conductivity models derived from previous studies. We can determine the sensitivity of such models to changes in the conductivity of particular layers, and use this as a guide in correcting the models to obtain a better fit to the observations.

6.1 *The superconducting core model*

In this model, the Earth is assumed to have a superconducting core of radius $a = q_0\,a_0$. The conductivity in the region $a < r < a_0$ is zero, and the solutions for the magnetic field are of the **U** type (equations (36) and (37)). The boundary condition $B_r = 0$ at $r = q_0\,a_0$ is applied, and the magnetic field at the surface $r = a_0$ can be calculated. For a zonal spherical harmonic of order n

$$\frac{i_n}{e_n} = \left(\frac{n}{n+1}\right) q_0{}^{2n+1}.$$

For the $P_1{}^0$ spherical harmonic

$$\frac{i_1}{e_1} = \frac{q_0{}^3}{2}. \tag{42}$$

The corresponding response W_1 is given by

$$W_1 = -(1-q_0^3)/(1+q_0^3/2).$$

The response is independent of frequency and the phase is 180° at all frequencies. The depth of the superconducting core is given by

$$q_0 = \{(1+W_1)/(1-\tfrac{1}{2}W_1)\}^{\frac{1}{3}}. \quad (43)$$

Such a model is incompatible with the observed response at low frequencies, where W_1 shows a marked frequency dependence. However, at frequencies between 0·05 and 0·25 c day^{-1} the response is fairly flat and the phase is close to 180°. The departures of the response from that predicted by theory can be seen more clearly by plotting the radius of the 'equivalent superconducting core' as a function of frequency. The equivalent superconducting core has a radius such that its response at a particular frequency is the same as that observed for the Earth.

Fig. 12 shows such a plot of core radius against frequency. Probably the best way of interpreting this curve is in terms of the current distribution at different frequencies. The superconducting core model is characterized by the current sheet at its surface. Possibly the radius of the equivalent superconducting core indicates the depth at which the majority of the current associated with a variation of a particular frequency flows. The fact that the penetration of this current does not change greatly between 0·05 and 0·25 c day^{-1} suggests a steep rise in conductivity. The radius of the superconducting core sets an upper limit of 500–600 km on the depth at which this rise occurs.

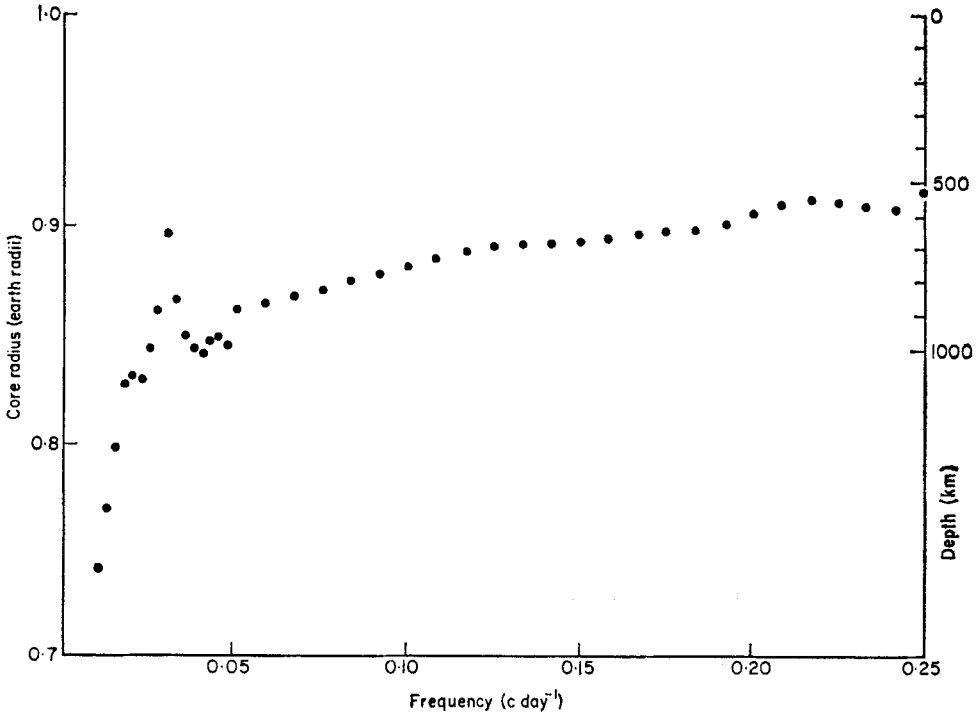

FIG. 12. Effective depth of superconducting core.

6.2 *The uniform core model*

Chapman & Price (1930) studied electromagnetic induction in a sphere of uniform finite conductivity. They calculated the response for a zonal harmonic of order n as

$$\frac{i_n}{e_n} = \left(\frac{n}{n+1}\right) q_0^{2n+1} \left\{1 - \mu\left[\frac{\kappa q_0 a_0}{(2n+1)} \cdot \frac{I_{n-\frac{1}{2}}(\kappa q_0 a_0)}{I_{n+\frac{1}{2}}(\kappa q_0 a_0)} + \frac{n(\mu-1)}{2n+1}\right]^{-1}\right\} \tag{44}$$

where $q_0 a_0$ is the radius of the uniform core, and $\kappa = \sqrt{(8\pi^2 \sigma f)}$. σ is the conductivity of the uniform sphere in e.m.u. and f is the frequency in c s^{-1}. $I_{n-\frac{1}{2}}$ and $I_{n+\frac{1}{2}}$ are modified spherical Bessel functions.

If we assume that $\mu = 1$, and only consider the P_1^0 response, equation (44) reduces to

$$Q_1 = \frac{i_1}{e_1} = \frac{q_0^3}{2}\left\{1 - \frac{3}{(\kappa q_0 a_0)} \cdot \frac{I_{\frac{3}{2}}(\kappa q_0 a_0)}{I_{\frac{1}{2}}(\kappa q_0 a_0)}\right\}. \tag{45}$$

Equation (45) should be compared with the corresponding expression for the superconducting core model—equation (42). The radius, qa_0, of the superconducting core model which has the same response at any frequency as the uniform core model is given by

$$\frac{q}{q_0} = \left\{1 - \frac{3}{\kappa q_0 a_0} \cdot \frac{I_{\frac{3}{2}}(\kappa q_0 a_0)}{I_{\frac{1}{2}}(\kappa q_0 a_0)}\right\}^{\frac{1}{3}} = F(\kappa q_0 a_0) \tag{46}$$

$x = \kappa q_0 a_0$ is a non-dimensional variable, so a single curve defines the dependence of q/q_0 on $\kappa q_0 a_0$. From the observations we can plot q as a function of

$$f = x^2/8\pi^2 q_0^2 a_0^2 \sigma.$$

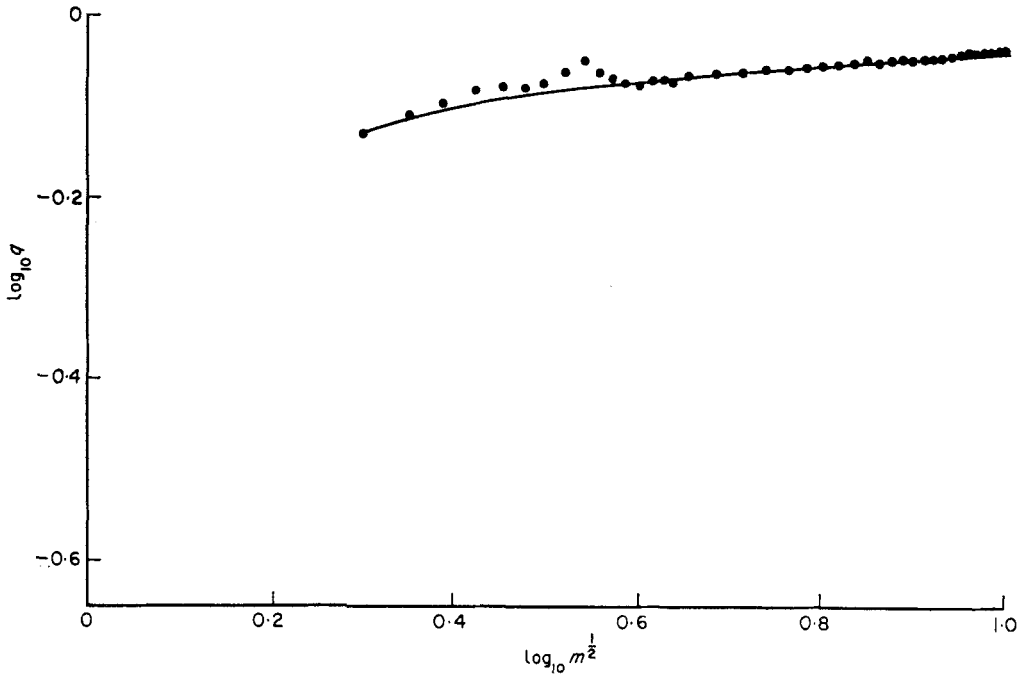

FIG. 13. Response of the uniform core model. Experimental data plotted as discrete points; theoretical curve is for $q_0 = 0{\cdot}94$, $\sigma = 0{\cdot}3$ mho m^{-1}. ($m = f/\Delta f$ where $\Delta f = 1/400$ c day^{-1}.)

By plotting $\log q$ against $\log f^{\frac{1}{2}}$ (determined experimentally) and comparing the result with $\log(q/q_0)$ plotted against $\log(\sqrt{q_0}\, a_0)$ (determined theoretically from equation (46)), we can test whether or not the observations fit the uniform core model. If they do, we can determine the values of q_0 and σ required for the best fit. Fig. 13 shows the result of such a comparison. The fit at high frequencies seems quite reasonable, but the slow variation of the function with frequency prevents us having too much confidence in the result. The uniform core model which best fits the data has the parameters $q_0 = 0{\cdot}94$, $\sigma = 0{\cdot}3$ mho m^{-1}, corresponding to a sharp rise in conductivity at a depth of about 400 km.

6.3 *Previous models of the conductivity distribution*

As a result of their work on the daily variation, Lahiri & Price (1939) suggested a distribution in which the conductivity rose steeply between 500 and 700 km from 10^{-3} mho m^{-1} to at least 1 mho m^{-1}. McDonald (1957) used the penetration of the secular variation through the mantle to estimate the lower mantle conductivity as approximately 100 mho m^{-1}. He joined this estimate to the upper mantle distribution of Lahiri & Price, and produced a conductivity model which will be referred to here as the Price–McDonald model (see Fig. 14).

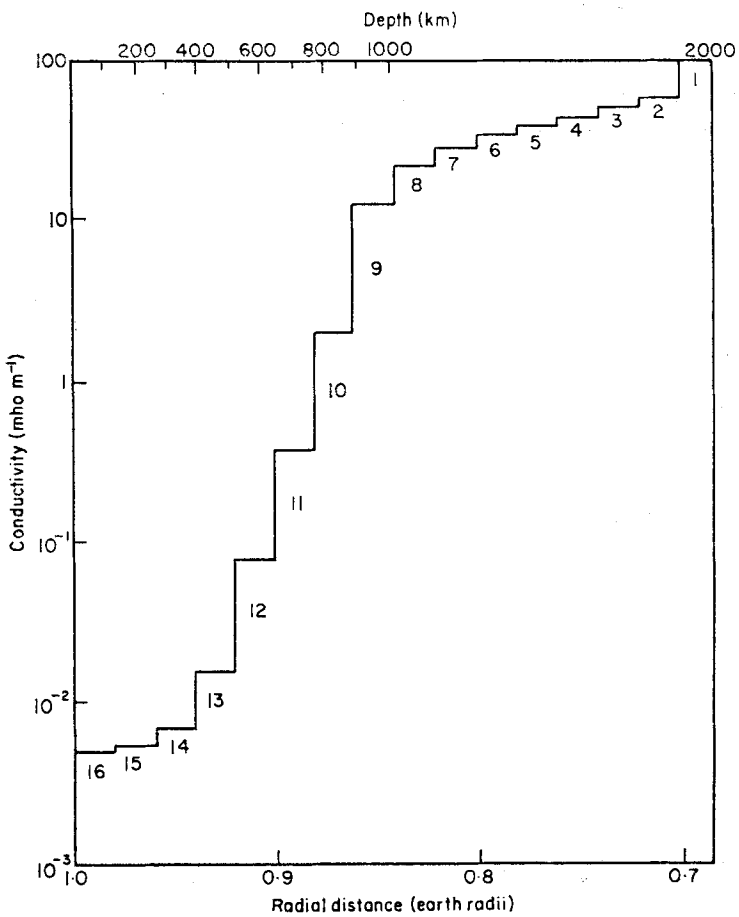

FIG. 14. Price–McDonald conductivity distribution as supplied to the computer program.

Using the techniques discussed in Section 5, the response of the Price–McDonald model was computed and compared with the observational data (Fig. 15). For this purpose the Earth was divided into shells of thickness $0{\cdot}02a_0$ and the bottom boundary was placed at $0{\cdot}7a_0$. The results indicate that there is a discrepancy between the observed and computed responses, particularly in the frequency range 0·05–0·25 c day^{-1}.

Taking the Price–McDonald distribution as the basic model, we can calculate the sensitivity of the response to changes in the conductivity of individual layers. Fig. 16 shows the perturbations in the response produced by increasing the conductivity of each layer by a factor of ten, the change being expressed as a percentage of the response of the basic model. From Fig. 16 we can see that, in the frequency range 0·01–0·25 c day^{-1}, the Price–McDonald model is most sensitive to changes in the conductivity of the layers in the vicinity of the rapid increase at 600 km. A reduction in the depth of the sharp rise would improve the agreement of the observed and theoretical response curves.

6.4 *The best fitting conductivity distribution*

A model which satisfactorily fits the modulus of the $P_1{}^0$ response is plotted in Fig. 17. The deep conductivity has been adjusted to fit the $P_2{}^0$ response at 1 c yr^{-1}, and the model has been simplified by introducing thicker layers where the conductivity varies slowly with depth.

6.5 *Errors in the conductivity distribution*

The discussion in Section 2.3 suggested that there were likely to be two main sources of error or uncertainty in any conductivity distribution derived from the

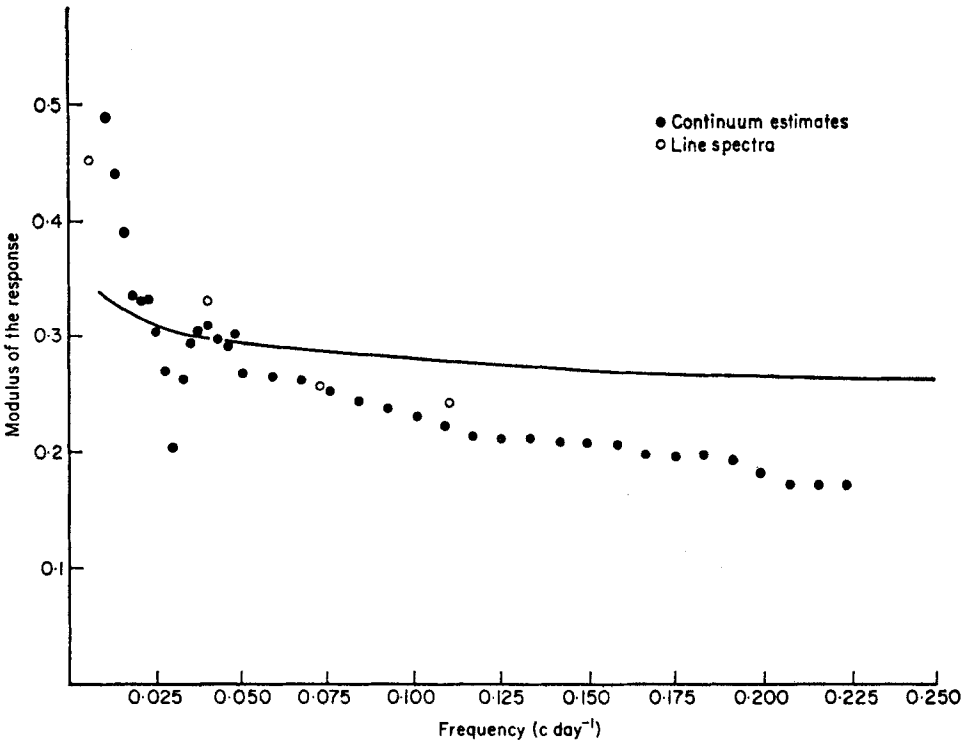

FIG. 15. $P_1{}^0$ response of the Price–McDonald model compared with the observations.

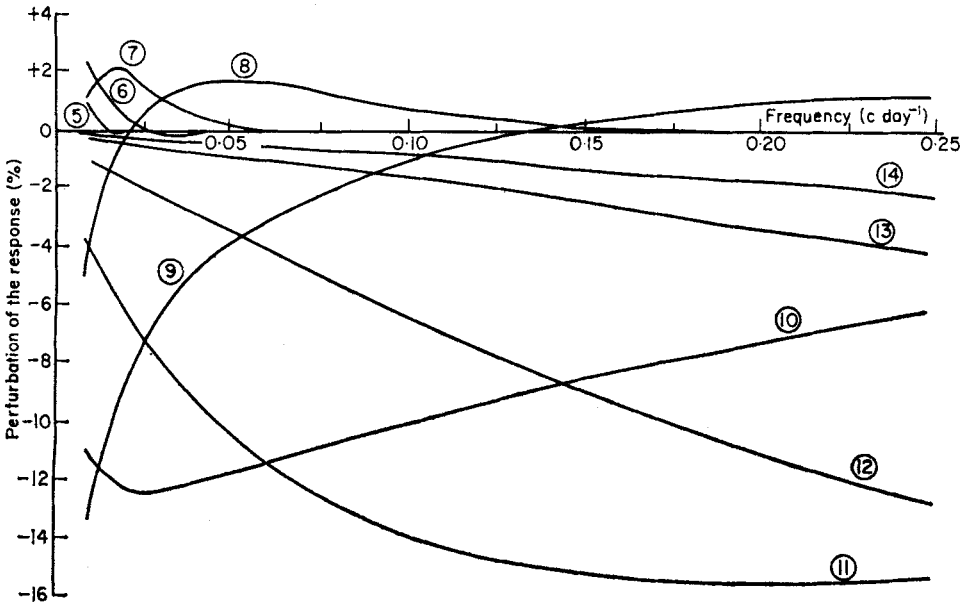

FIG. 16. Perturbations in the P_1^0 response of the Price–McDonald model. Numbering of curves corresponds to layer numbers in Fig. 14.

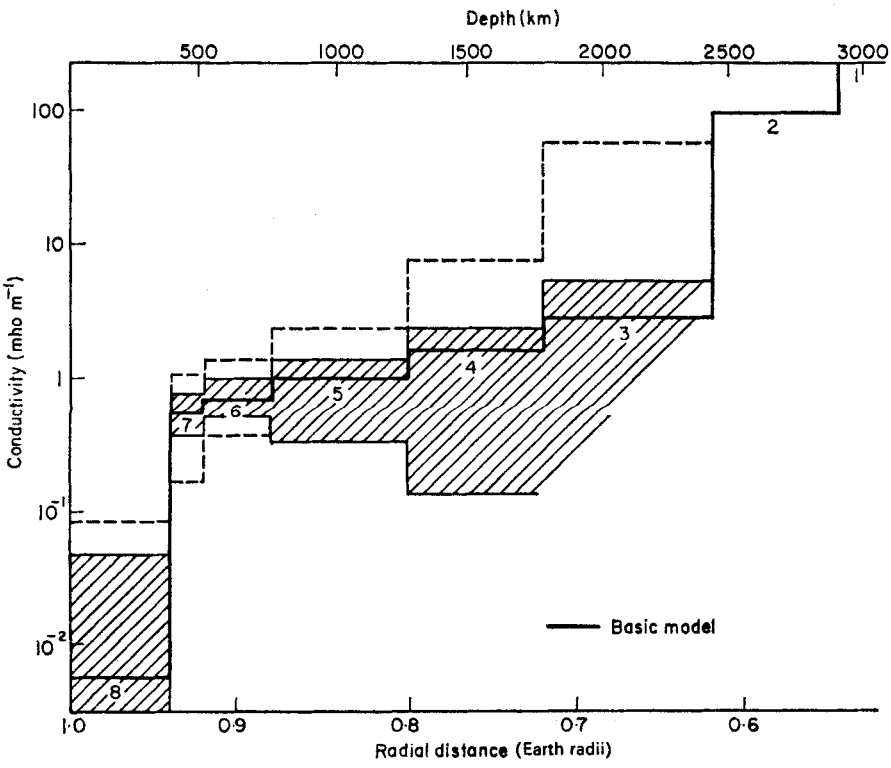

FIG. 17. Range of conductivity models compatible with the response measurements. Shaded area corresponds to ±1 standard error, dashed lines to ±2 standard errors.

available observational data. The first source of error lies in the departures of the real data from that required for a unique determination of the conductivity distribution. In addition, uncertainties are introduced by measurement errors in the response curve.

Of the first type of error, the most serious is that arising from the limitations on the frequency range, in particular the neglect of the high frequency end of the spectrum. Highly conducting layers at depths between 0 and 400 km may shield deeper layers from the long period magnetic variations. A rough estimate of the effect of the oceans can be made by supposing their effect to be equivalent to that of a uniform shell of thickness 1 km and conductivity 3 mho m^{-1} (Lahiri & Price 1939). The perturbation of the P_1^0 response of the newly-determined conductivity model, caused by such a modification, is less than 2 per cent at 0·25 c day^{-1}—well within experimental error. At depths of 30–100 km, the conductivity may locally reach 1 mho m^{-1}; however, not enough is yet known about the distribution of such regions to be able to assess their effect on the response.

Errors of measurement may, to some extent, include the uncertainties discussed in the previous paragraph. Some attempt should be made to investigate the range of models which is compatible with a deviation of one or two standard errors from the response estimates. One approach to this problem is to use Monte Carlo methods (Press 1968). However, the method adopted here is to examine the variations in response associated with changes in the conductivity of a particular layer, and to reject values of the conductivity of that layer which produce values of the response outside the limits of experimental error. In Fig. 18 the P_1^0 response of the basic model is plotted as a function of the conductivity of layer 6 (see Fig. 17), for a number of frequencies. The response of the basic model and the error limits are

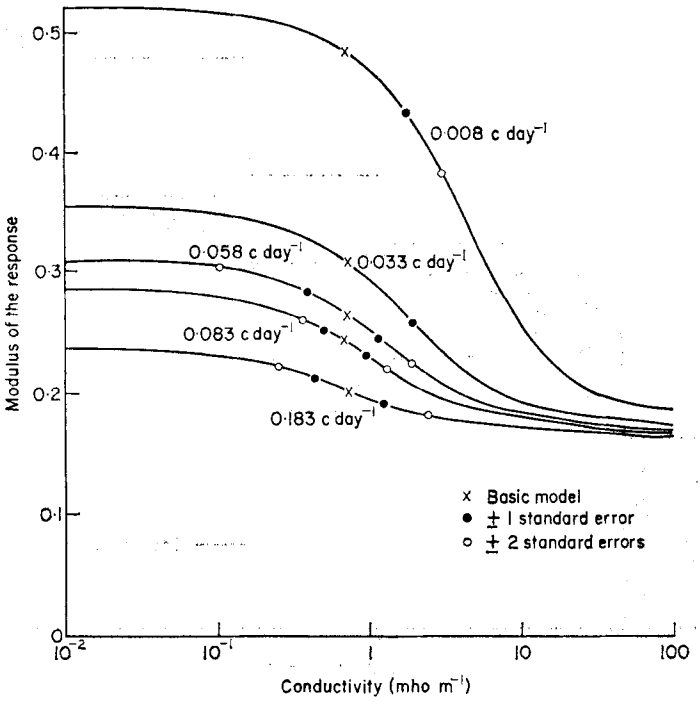

FIG. 18. Dependence of P_1^0 response of basic model on conductivity of layer 6, for different frequencies.

plotted, and the corresponding limits of conductivity can be read off. Some frequencies set closer limits on the conductivity of a particular layer than others; for layer 6 the most sensitive frequency is 0·083 c day^{-1}.

By using this technique, limits can be set on the whole of the conductivity distribution (Fig. 17). The question arises of whether or not such a method of calculating errors is valid. A positive change in the response associated with a decrease in the conductivity of one layer might be balanced by a negative perturbation caused by an increase in the conductivity of some other layer. This again raises the problem of uniqueness. Even if we suppose that an exact response function determines a unique conductivity distribution, it does not follow that any equivalent result holds when the response is not exactly determined. The method described here can only set very tentative limits on the range of conductivities compatible with the observations.

7. The significance of the conductivity distribution

7.1 *Comments on the distribution*

A smoothed version of the conductivity model derived in Section 6 is plotted in Fig. 19, together with the distributions of other investigators. The range of distributions shown corresponds to two standard errors uncertainty in the measured response, and provides a basis for comparison with the other models.

It is evident from Fig. 19 that frequencies in the range 0·01 to 0·25 c day^{-1} can tell us little about the conductivity of the top 400 km of the Earth. Any conductivity less than 0·1 mho m^{-1} is compatible with the observations. In a sense this is just as well, because local regions of high conductivity are believed to occur in the uppermost part of the mantle.

At about 400 km the conductivity increases by approximately two orders of magnitude to a value of 1 mho m^{-1}. The jump is completed within 200 km or so.

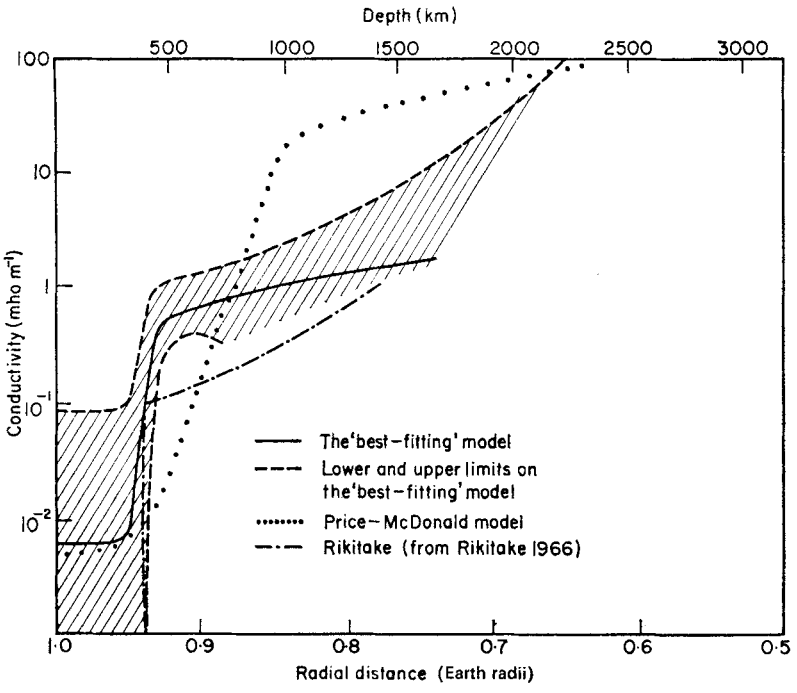

FIG. 19. Electrical conductivity of the upper mantle.

From the point of view of the depth and size of this jump, the new model appears to agree rather better with Rikitake's distribution than with that of Price & McDonald. At depths of 500 km or more, the conductivity levels off and continues to increase more slowly. At depths greater than 1200 km the uncertainty becomes too great for the model to do more than set an upper limit on the conductivity.

Previous work on the secular variation (McDonald 1957) has suggested that the conductivity at the bottom of the mantle lies in the range 10–1000 mho m^{-1}. This study does not contradict McDonald's findings, as it only provides reliable information about conductivity at depths of less than 1000 km or so.

7.2 *Laboratory measurements of conductivity*

Conductivity distributions such as those shown in Fig. 19 can be interpreted in terms of the effects of temperature, pressure, and phase on the conductivities of likely mantle materials. Tozer (1959) has discussed the relevant laboratory experiments on the effects of temperature and pressure on conductivity. He concludes that, in the mantle, the dominant mode of conduction is that of intrinsic semiconduction. Ionic conduction is believed to be suppressed by the high pressure (see also Lubimova (1967)). Within the mantle, the temperature dependence of conductivity can be expressed by the equation

$$\sigma = \sigma_0 \exp -E/2\kappa_0 T \tag{47}$$

where σ_0 has a value in the range 100–500 mho m^{-1} for magnesium-rich olivines, and E is about 3eV (κ_0 is Boltzmann's constant, T the absolute temperature).

Another factor, of critical importance, is that of composition. The upper mantle is believed to consist very largely of members of the olivine series of solid solutions. Olivine has the general formula $(Mg, Fe)_2 SiO_4$; its composition can range from forsterite (Mg_2SiO_4) to fayalite (Fe_2SiO_4). Hamilton (1965) summarizes in a diagram the effects of iron content on the conductivity of olivines. There is a difference of at least five orders of magnitude between the conductivities of forsterite and fayalite at the same temperature. Fortunately, the upper mantle is believed to be reasonably homogeneous chemically (Clark & Ringwood 1964), with peridotite (approximate composition $(Fe_{0\cdot1} Mg_{0\cdot9})_2 SiO_4$) the most likely constituent.

However, a phase change from the olivine to the spinel structure is believed to occur in the mantle transition region between 400 and 900 km. Akimoto & Fujisawa (1965) have investigated the effects of an olivine–spinel phase transition on the electrical conductivity of fayalite, and find a discontinuous increase of some two orders of magnitude associated with the transition. It seems likely that a similar conductivity jump will occur in peridotite; however, because the system has more than one component, the rise will be more gradual.

7.3 *Interpretation of the conductivity distribution*

As a first step in the interpretation of the conductivity model, we can assume that the variation with depth is caused by the effect of increasing temperature, as given by equation (47). Knowing E and σ_0 from laboratory measurements, we can estimate the temperature $T(r)$ by inverting equation (47). The results of such a calculation, based on the figures given by Tozer for E and σ_0 of peridotite, are plotted in Fig. 20 as T_{max} (olivine) and T_{min} (olivine), corresponding to the upper and lower limits of conductivity. At depths less than 300 km, Tozer's own temperature curve is plotted. Fig. 20 shows that, if the mantle is assumed to be uniform, there must be a discontinuity in the temperature gradient at 400 km.

The other possibility is a change in σ_0 or E. The most likely explanation seems to be a change in E brought about by an olivine–spinel phase transition. Akimoto & Fujisawa (1968) have carried out experiments on such a transition in solid solutions

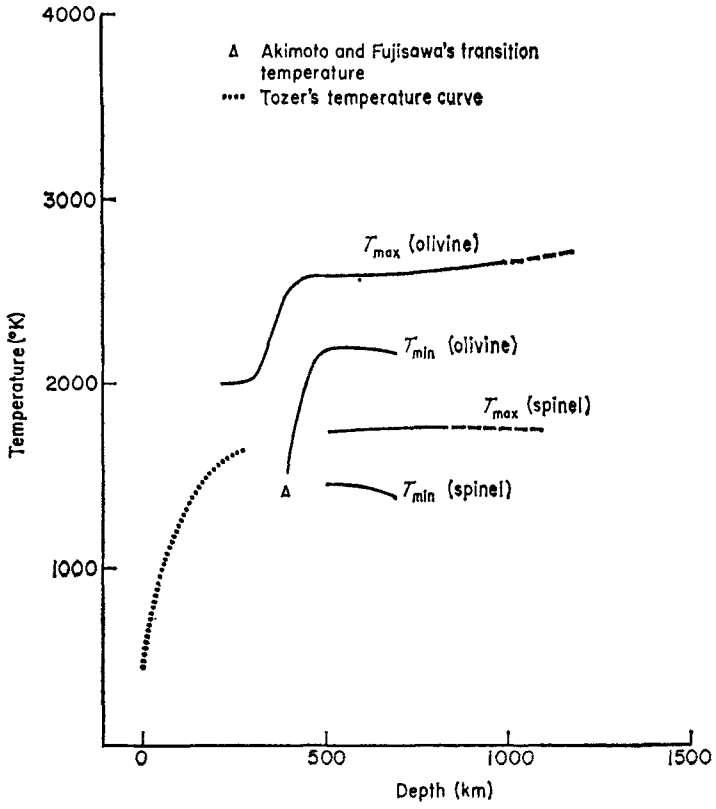

FIG. 20. Temperatures in the upper mantle.

of forsterite and fayalite. The depth at which the transition would occur, assuming a peridotite mantle, is controlled by the temperature. Akimoto & Fujisawa believe that the phase change can be correlated with a rapid increase in seismic velocity that has been reported at depths of around 370 km by Niazi & Anderson (1965) and others. On this assumption, the width of the transition would be 50–80 km, and the temperature would be about 1420°K. The conductivity model appears to agree quite well with such an interpretation, particularly in view of the experiments of Akimoto & Fujisawa on the conductivity jump associated with the olivine–spinel transition in fayalite.

We can now revise the temperature estimates for depths greater than 400 km. Unfortunately E and σ_0 are not known for the spinel form of peridotite. McKenzie (1967) suggests that it might be reasonable to take σ_0 (olivine) = σ_0 (spinel), and the ratio E (spinel)/E (olivine) for peridotite to be the same as for fayalite, which is known. The temperature curves T_{max} (spinel) and T_{min} (spinel) of Fig. 20 were computed on this basis. It is encouraging that the resultant temperature profile is reasonably smooth, and also agrees with Akimoto & Fujisawa's transition temperature.

8. Conclusions

The conductivity distribution derived from measurements of magnetic variations in the frequency range 0·01 to 0·25 c day^{-1} appears to be consistent with the effects of temperature and pressure on a semiconducting mantle composed of magnesium-rich olivine, provided allowance is made for an olivine–spinel phase transition at a depth of 400 km.

There is a good deal of scope for the improvement of the conductivity determination. The data that was used in this analysis was rather limited, and it should prove possible to reduce the limits of error assigned to the response measurements quite considerably. More work is required on the determination of E and σ_0 as functions of temperature and pressure; also experiments to confirm the existence of a conductivity jump associated with the olivine–spinel transition in peridotite.

The uncertainty in temperature distributions derived by other methods increases the importance of investigations of the electrical conductivity.

Acknowledgments

The work described in this paper was carried out at the Department of Geodesy and Geophysics of the University of Cambridge. I should like to thank Sir Edward Bullard for his advice and encouragement, and Dr R. L. Parker who suggested the matrix method of programming the theoretical response calculations and made many other helpful comments. Dr B. R. Leaton of the Royal Greenwich Observatory kindly supplied me with digitised records of the magnetic fields at Greenwich and Abinger. The computations were performed on the I.B.M. 7090 computer at Imperial College, London, and on the 360/44 computer of the Institute of Theoretical Astronomy at Cambridge.

Department of Environmental Sciences,
University of Lancaster.

1969 *February.*

References

Abramowitz, M. & Stegun, I. A., 1965. *Handbook of Mathematical Functions*, Dover, New York.
Akimoto, S. & Fujisawa, H., 1965. *J. geophys. Res.*, **70,** 443.
Akimoto, S. & Fujisawa, H., 1968. *J. geophys. Res.*, **73,** 1467.
Anderson, D. L., 1965. *Phys. Chem. Earth*, **6,** 1.
Banks, R. J. & Bullard, E. C., 1966. *Earth Planet. Sci. Lett.*, **1,** 118.
Blackman, R. B. & Tukey, J. W., 1958. *The Measurement of Power Spectra from the Point of View of Communications Engineering*, Dover, New York.
Cahill, L. J., 1966. *J. geophys. Res.*, **71,** 4505.
Chandrasekhar, S., 1961. *Hydrodynamic and Hydromagnetic Stability*, Appendix 3, Oxford University Press.
Chapman, S. & Price, A. T., 1930. *Phil. Trans. R. Soc.*, **A229,** 427.
Chapman, S. & Bartels, J., 1940. *Geomagnetism*, Chap. 12, Oxford University Press.
Clark, S. P. & Ringwood, A. E., 1964. *Rev. Geophys.*, **2,** 35.
Coleman, P. J., Davis, L., Smith, E. J. & Jones, D. E., 1966. *J. geophys. Res.*, **71,** 2831.
Currie, R. G., 1966. *J. geophys. Res.*, **71,** 4579.
Currie, R. G., 1968. *J. geophys. Res.*, **73,** 2779.
Eckhardt, D., Larner, K. & Madden, T., 1963. *J. geophys. Res.*, **68,** 6279.
Frank, L. A., 1966. *J. geophys. Res.*, **71,** 4631.
Hamilton, R. M., 1965. *J. geophys. Res.*, **70,** 5679.
Johnson, F. S., 1961. *Satellite Environment Handbook*, Chap. 1, Stanford University Press.
Lahiri, B. N. & Price, A. T., 1939. *Phil. Trans. R. Soc.*, **A237,** 509.
Lubimova, E. A., 1967. *The Earth's Mantle*, ed. by T. F. Gaskell, Chap. 10, Academic Press, New York.
McDonald, K. L., 1957. *J. geophys. Res.*, **62,** 117.

McKenzie, D. P., 1967. *International Dictionary of Geophysics, The Earth's Mantle*, ed. by S. K. Runcorn, Pergamon, Oxford.
Munk, W. H. & Cartwright, D. E., 1966. *Phil. Trans. R. Soc.*, **A259,** 64.
Niazi, M. & Anderson, D. L., 1965. *J. geophys. Res.*, **70,** 4633.
Parker, E. N., 1962. *Space Sci. Rev.*, **1,** 62.
Press, F., 1968. *J. geophys. Res.*, **73,** 5223.
Rikitake, T., 1966. *Electromagnetism and the Earth's Interior*, Elsevier, Amsterdam.
Stratton, J. A., 1941. *Electromagnetic Theory*, McGraw-Hill, New York.
Swisher, R. L. & Frank, L. A., 1968. *J. geophys. Res.*, **73,** 5665.
Tozer, D. C., 1959. *Phys. Chem. Earth.*, **3,** 414.
Wilcox, J. M. & Ness, N. F., 1965. *J. geophys. Res.*, **70,** 5793.